Unstable Temperature Distribution in Friction Stir Welding

Sadiq Aziz Hussein[a, b], S. Thiru[a,*], Abd Salam Md Tahir[a], R. Izamshah[a]

[a] University Teknikal Malaysia Melaka (UTeM), Melaka, Malaysia.
[b] Foundation of Technical Education, Baghdad, Iraq.
thiru@utem.edu.my

Abstract

In the friction stir welding process, a non-uniform and high generated temperature is undesirable. Unstable temperature and distribution affects thermal and residual stresses along the welding line, thus necessitating mitigation. This paper presents a simple method to prevent significant temperature difference along the welding line and also to help nullifying some defect types associated in this welding, such as; end-hole, initial un-welded line and deformed areas. In the experimental investigation, a heat and force thermocouple and dynamometer were utilized while couple-field thermomechanical models were used to evaluate temperature and its distribution, plastic strain, and material displacement. The suggested method generated uniform temperature distributions. Measurement results are discussed, showing a good correlation with predictions.

Key words: *Friction stir welding, unstable temperature distribution, start-plunge and end-hole defects, tool backup plate, thermomechanical model.*

1. Introduction

Friction stir welding (FSW) is becoming more widely used as a manufacturing alternative in aviation, marine, and auto applications [1]. When fusion welding is used to weld Al alloys, low tensile and fatigue strength are obtained because of the associated defects, residual stresses, and material solidification [2]. Therefore, solid-state joining methods, such as the recently developed FSW, efficiently join similar or dissimilar Al alloys [1, 2]. However in FSW, certain associated defects have to be eliminated, and non-uniform temperature distributions along the welding line should be mitigated.

Heat generated by the FSW process is important in plasticizing the material locally below the tool shoulder. Therefore, several numerical models have been used in the literature to evaluate the resultant experimental temperature. For instance, Frigaard et al. [3] developed a thermal model and addressed the brief transition of heat gradients below the shoulder along the thickness direction in four different forms. Furthermore, plunging and dwell time (DT) generate the maximum temperature, which decreases while the tool moves along the welding line [4]. Therefore, temperature is varies during the FSW process perpendicularly through the work-piece thickness as well as longitudinally and transversely along the weld centerline, which results in various evolutions of microstructure and hardness [2]. Moreover, high temperature in FSW and friction stir processing (FSP) may be undesirable [5, 6]. Thus, there is a need for more studies investigating the stability of the resultant temperature.

Despite its many significant advantages [7], this welding type also has several defects. End-hole defect and plunging site position may decrease the length of the plate (L) to a shorter length (L_n), as shown in Fig. 1. A hole in the plate generally results in a high mechanical stress intensity factor, which may induce cracks [8, 9]. Therefore, four suggested methods aimed at eliminating end-hole defects through run on/off tabs, plugs, retractable pin tools, and the relocation of the end-hole are available in the literature [10]. Huang et al. [11] recently used a different method that adopts the principle of friction fill spot weld. After an aluminium pin is consumed into the end-hole, the resultant flat steel shoulder enhances the mechanical properties by employing FSP along the welding line [11]. It is clear that some difficulties may arise during the implementation of these methods.

This study investigates temperature instability in FSW, as well as determines whether heat varies as a result of tool movement [4] or tool motion away from the plate edge. This work also suggests a time- and cost-efficient technique to prevent some certain defects. A thermochemical model was developed to validate thermocouple results and to determine the appropriate plunging site distance from the plate edge.

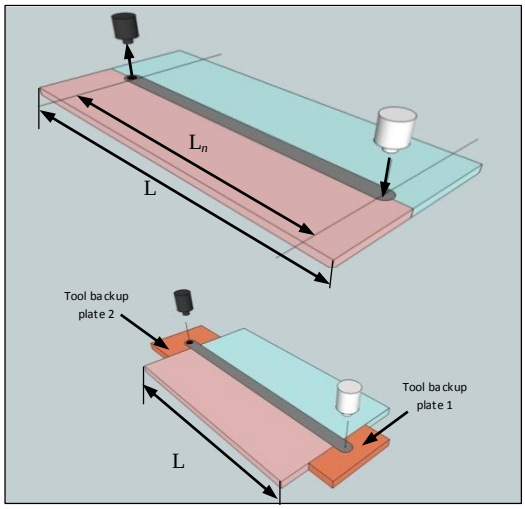

Fig. 1, Schematic of the FSW process.

2. Experimental procedure

In the experiment, aluminum alloy 6061-T6 (AA6061-T6) plates (300 mm × 200 mm × 6.4 mm) were used. The chemical compositions and ultimate tensile strengths of these plates are shown in Table 1. The tool was fabricated from hardened (JIS SKD61) tool steel. The tool was smoothly cylindrical, and its dimensions are as follows: shoulder diameter, 12.2 mm; pin diameter, 5.2 mm; and pin length, 3.5 mm. The tilt angle of the rotating tool with respect to the *Z*-axis was 0°, and the shoulder surface was straight. In this study, FSP was utilized because this method generates heat and force similar to those of FSW [7]. Moreover, FSP is more efficient than FSW in terms of time and clamping. The tool was plunged into the mid line of the work-pieces. To reduce the initial plunging forces for the safety of the machine, plunge speed (head feed) was set at only 5 mm/min. Rotational speeds were 500 and 1000 rpm, and a CNC milling machine (HASS VF-1D) was used as the welding machine.

Table 1: Chemical composition of alloy elements in the 6061-T6 plates

Chemical composition (wt%)										Ultimate tensile strength (MPa)
Mg	Si	Mn	Cu	Fe	Cr	Zn	Ti	Other	Al	312±10
1.06	0.67	0.014	0.23	0.32	0.21	0.007	0.02	0.05	Bal	

As shown in Fig. 2, a 0.1 kgf resolution dynamometer was fixed on the CNC table to measure the values of the forces needed for modeling. The dynamometer was adjusted to determine the forces in the *Z*-direction. A low-carbon steel plate was placed between the dynamometer and the work-pieces as a backup. Holes with 1.5 mm diameter were drilled at strategic positions to measure the temperature by using a thermocouple with eight ports, as presented in Fig. 3. The shoulder mainly generates heat [3]. Thus, the first port was fixed on the material around the edge of the shoulder. To investigate the effect of the plunging distance of the first pin from the plate edge on peak temperature and edge deformation, distances x_1 were set at 30, 55, and 80 mm, as shown in Fig. 2. The influence of 5, 10, 20, and 40 s DTs were also determined in this study.

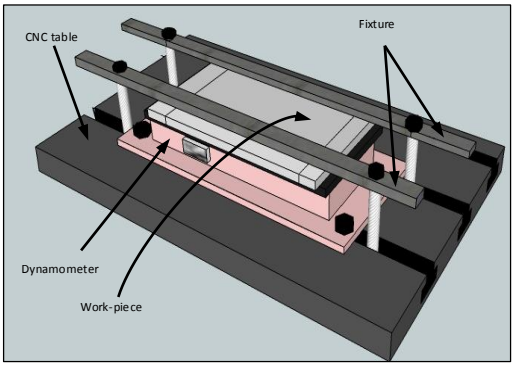

Fig. 2, Schematic diagram for experimental work requirements.

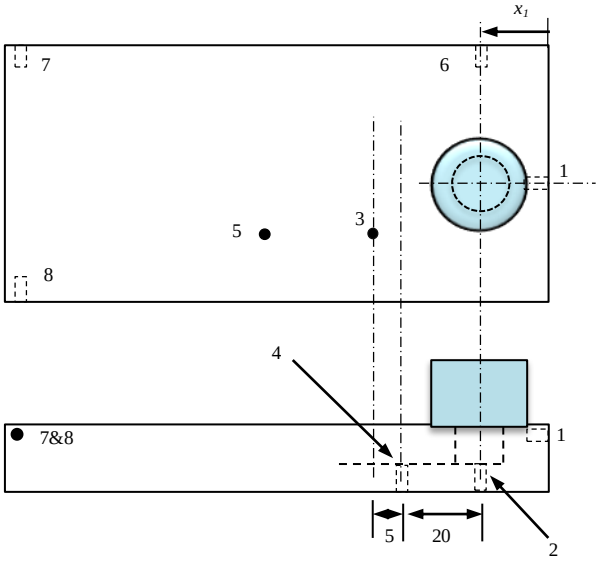

Fig. 3, Positions of holes on the plate for thermocouple temperature measurement.

3. Finite element model (FEM)

In this study, an adopted sequentially coupled model was divided into two parts. The first part was to evaluate the temperature and its distribution, whereas the second part was to indicate the adaptive plastic deformation and material displacement. A 3D coupled field (multi-physics) model was generated using ANSYS14 software. In thermal analysis, the SOLID278 element was utilized, whereas SOLID185 was used in structural analysis. The heat generated by the tool was simulated at the penetration zone, this indicating both pin plunge and DT effect on the plastic deformation and material displacement at the plate edge. Stirring was not modeled, because, incorporating this effects on plastic deformation and material displacement is difficult. To ensure the model accuracy, the temperature values obtained from FEM results were first compared with those obtained through experimentation. The thermal history was then considered in the structural model. This model was complicated by the effect of nonlinear heat distribution effect on material behavior, which depends on whether the model behaves as elasto-plastic or viscoplastic. In this study, it is assumed that the tool is rigidly solid and the work-piece is a ductile material composed of multi-linear, kinetic hardening elasto-plastic [12]. Also, stress–strain curves of AA6061-T6 for various temperatures were adopted [12]. To improve modeling accuracy, a fine mesh was applied at the tool/work-piece interface. Calculation time was reduced by adopting one half of the model due to the symmetry. The boundary conditions (BC) at the top and bottom of the work-pieces (conduction and convection) affects the results, hence; this study adopted the BC applied by Mun and Seo [13]. Heat generation is changes according to the contact area (pin/shoulder), which produced different forces until a specific length of the shoulder (0.2 mm) dipped inside the work-piece for a period of time (DT). Given this difficulty in simulation, individual average force values were used with respect to pin penetration and DT, as discussed in subsequent sections.

In FSW, heat is mainly generated by friction and plastic deformation. In the literature, some formulae were developed to evaluate the influence of FSW/FSP parameters on the extent of heat generation within the welding/processing area. Many heat analytical models were also established, including the 3D models [3, 14]. The pin may generate only 2% heat [15]; thus, it is neglected in most studies. Equation 1 represents heat generated by the shoulder [3]. The same equation was used to compute the heat produced by the pin after the shoulder diameter is converted into the pin diameter for heat generation by pin plunging process.

$$Q = (4/3)\pi^2 \mu\omega P R^3 \quad (1)$$

where Q, μ, ω, P, and R are the generated heat (Watt), friction coefficient, rotational speed in (rev/sec), pressure (N/m^2), and shoulder or pin diameter (m), respectively.

In FSW/FSP, the heat generated by the first touch of the pin which increases the heat of the plate before the shoulder dips inside. Moreover, the material begins to plasticize in that area. Thus, the heat generated by the pin is very important in the initial welding stage (plunging), the shoulder increases this heat, especially during DT.

The heat decreases when the tool is moved, also it was reported that accelerating weld speed lowers temperature [4, 16]. This phenomenon may be related to the short conduction time between the tool and the work-piece materials. Thus, the amount of heat at the plunging and dwelling represents the peak value during the welding process. The transient heat transfer equation can be written as

$$\rho C_p \frac{\partial T}{\partial t} = k\left(\frac{\partial^2 T}{\partial x^2} + \frac{\partial^2 T}{\partial y^2} + \frac{\partial^2 T}{\partial z^2}\right) + Q_i \tag{2}$$

where ρ, C_p, t, k, and Q_i are the densities, specific heat, times, thermal conductivities, and the internal heat generation rates in the three axes, respectively.

Zhu and Chao [17] assumed that the thermomechanical model follows the yield criteria developed by von Mises. Their model confirmed the occurrence of transient behavior and the relationship between the stresses σ_{ij} and strain εij in their study was defined by

$$\dot{\varepsilon}_{ij} = \frac{1+v}{E}\dot{\sigma}_{ij} - \frac{v}{E}\dot{\sigma}_{kk}\delta_{ij} + \lambda s_{ij} + \left[\alpha + \frac{\partial \alpha}{\partial T}(T - T_o)\right]\dot{T} \tag{3}$$

where E, v, and α are the modulus of elasticity, Poisson's ratio, and thermal expansion coefficient in $s_{ij} = \sigma_{ij} - \left(\frac{1}{3\sigma_{kk}\delta_{ij}}\right)$, respectively. This equation represents the components of deviatoric stresses. λ, T_o, and $\dot{(\,)}$ denote the plastic flow factor, room temperature, and time differences.

Strain rate ($\bar{\varepsilon}$) affects friction coefficient (μ) [18]. This phenomenon was reported in many studies, including that of Soundararajan et al. [19], who used a range of μ. Other researchers have applied constant values of μ to estimate the all-inclusive influence of both thermal and plastic factors on the FSW process [12, 20]. In the present study, the variation in the physical material properties of the AA6061-T6 plates were adopted from the study of Nandan et al. [4] with respect to temperature, specific heat (C_p), and thermal conductivity (k). Furthermore, a constant friction coefficient of μ = 0.4 was implemented in the model.

4. Results and model validation

The thermocouple results are in good agreement with those established in [4]. At the penetration stage, Fig. 4 clarifies the temperature increments relative to time. Rotational speed was the main contributor to this increament. For example, the temperature significantly increased at the 10th s (≈ 85 °C) between 500 and 1000 rpm, as exhibited in Fig. 4. Moreover, Fig. 5 indicates that pin-generated heat is dominant at the penetration stage and the heat slightly increases when the shoulder touches the work-pieces and dips. To determine the importance of the heat generated by the pin, the experiments were stopped with 10 mm movement along the welding line. Figure 5 shows that the stirring zone temperature (pin zone) remained higher than that of the shoulder (ports 2 and 1 for the plunging stage, and ports 4 and 3 for the tool transition stage). This finding may be related to convection and radiation, which decreases the heat at the shoulder rim.

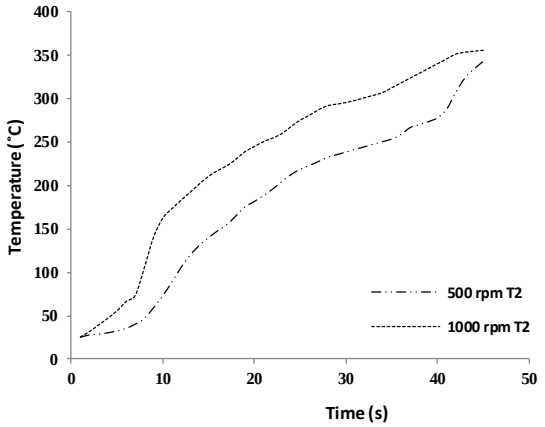

Fig 4, Penetration temperature values (pin and shoulder) for different rotational speeds.

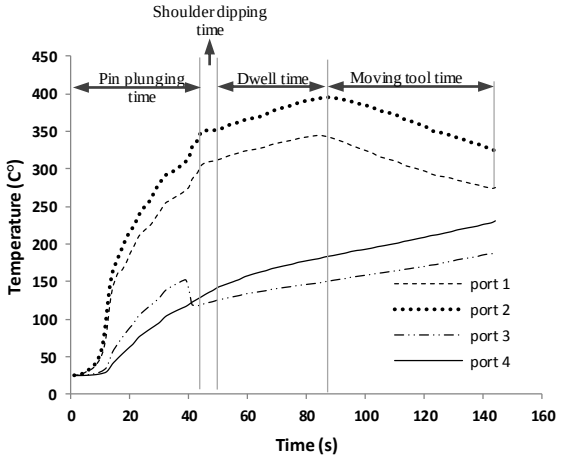

Fig 5, Temperature values and distribution at ω = 1000 rpm, DT = 5 s—40 s. Ports 5, 6, 7, and 8 were neglected (no significant change).

In the first two stages of FSW, heat generation was difficult to simulate based on Eq. 1 because of the changing force values and heat generation sources (either pin or shoulder). Thus, the average force readings (F_{ave}) values of the dynamometer were used to model the effect of plunging and DT separately. The experiments conducted at 500 rpm generate extremely strong forces, which may damage the dynamometer and the machine. Thus, this study considers only the temperature measured at this rotation speed. These strong forces were also reported in several studies [19, 20, and 21] at rotational speeds of 450–400, 344, and 500 rpm. These strong forces are related to the strain hardening of the material, that is, as the temperature exceeds the recrystallization point, strain hardening decreases [22] and the forces weaken.

On the edge of the work-piece, temperature measurement was problematic as a result of severe deformation, which dislodged the thermocouple ports at the connection points at different values of x_1 (30, 55, and 80 mm). However, in the FEM model a range of x_1 were simply used to investigate this effect on temperature instability.

When the rotation and penetration speeds were 1000 rpm and 5 mm/min respectively, the pin fully penetrated the work-piece after 42 s, and the actual measured temperature was 339 °C (as shown in Fig. 5). In the penetration stage, the error in the results with respect to simulated temperature (Fig. 6) was 11.2%. This error may be related to the transient nature of the effective forces considered and/or the effect of the cylindrical surface of the pin on the modeling process, such effect was neglected.

To determine the effect of DT, Fig. 7 depicts the thermocouple temperature values for two different times. The differences among temperature values are constant, and no contribution effect was observed on the three values selected relative to plunging distance from the plate edge (x_1 distance). The percentage error between the experimental and the numerical results were minimal at DT 20 s, as presented in Fig. 8 at the selected x_1 distances. From the heat process model which selected for this study, the predicted temperature and its distribution accuracy were in a reasonable range. The accuracy increased the confidence level of the model results and the effect of the plunging position on temperature. The distribution is shown in Fig. 9. Furthermore, peak temperature was high at the edges of the plate when the tool penetrated the area near these edges (Figs. 9 and 10). As indicated in Fig. 9, the simulated temperature values were inaccurate when DT was short (less than 5 s) because the heat generation source is rapidly changes from the pin to the shoulder. The result in Fig. 10 is related to the small convection area around the tool, and the conduction area is insufficient to conduct heat to the backup plate. Chao et al. [23] examined the parameters that affect the amount of conducted heat, surface condition, and the effect of contact pressure on temperature. When the penetration point was far from the edge, the convection and conduction areas were large. Therefore, the temperature was low, and its distribution was in equilibrium. As previously discussed, the distance of tool penetration from the plate edge (x_1) significantly affects temperature stability. This variation in temperature is reported in the literature [4, 16] and has often been associated only with weld speed. However, the distance of the tool from the plate edge must also be ascertained.

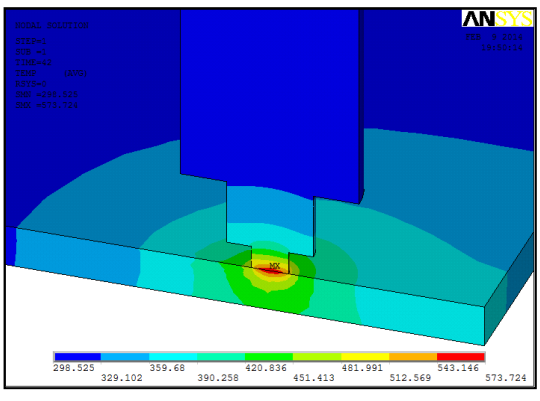

Fig. 6, Temperature contour gradient of the whole pin penetration stage. (Temperature is in Kelvin).x_1=30mm.

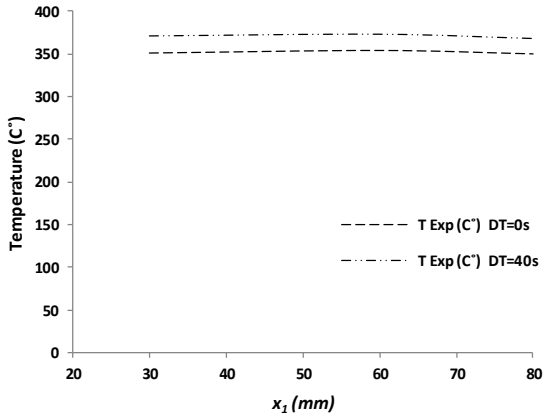

Fig. 7, Thermocouple results for different distances (x_1) and DT.

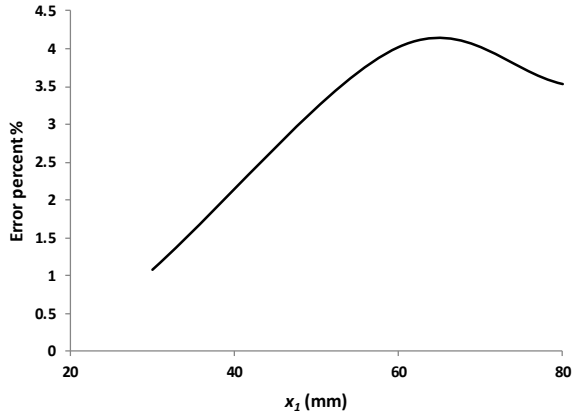

Fig. 8. Error between experimental and FEM results for ω=1000 rpm, (DT=20s).

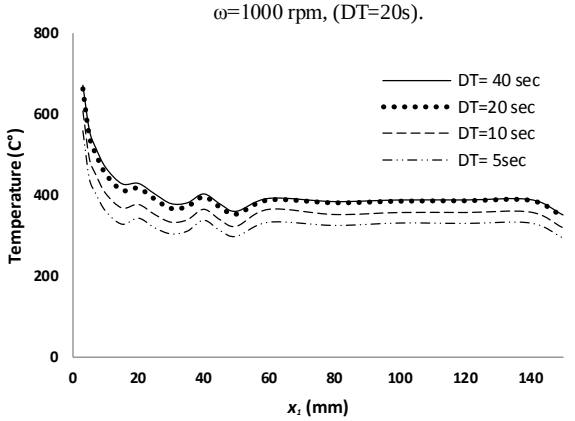

Fig. 9, Simulated temperature values for different plunge distance from the edge

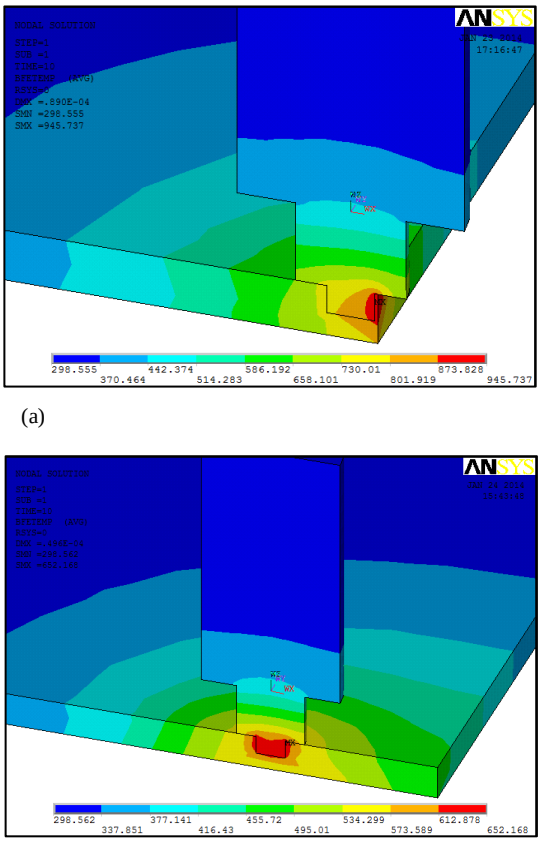

Fig.10, Temperature contours results of FEM simulation. (DT= 40 s and temperature is in Kelvin). (a) x_1 = 3 mm, (b) x_1 = 30 mm. The temperatures values are in Kelvin.

The literature references a weak joint that can be resulted in case of long DT, which lead to an overheating [24]. The melting temperature (T_m) of the AA6061-T6 plates was set at 625 °C. At 500 and 1000 rpm, all resultant temperatures for different DT values were below 80% of T_m. These temperatures do not correspond to overheating. In this study, the DT periods were 5, 10, 20, and 40 s. Table 2 shows the average values of the forces at these different periods. The experimental temperature values and distribution induced transient heat transfer in the first two stages of FSW. The simulated heat at 1000 rpm and x_1 = 30 mm agrees with that produced experimentally given 5 s to 40 s DT, as presented in Fig. 11.

Table 2: Experimental and numerical temperature results for 1000 rpm and different dwell time.

Average F (kgf)	Q (w)	T Exp. (˚C)	T FEM (˚C)	DT (sec)
306 (3002N)	624.94	395	379	40
330 (3233N)	673.03	371	367	20
334 (3277N)	682.19	360	333	10
348 (3414N)	710.71	351	304	5

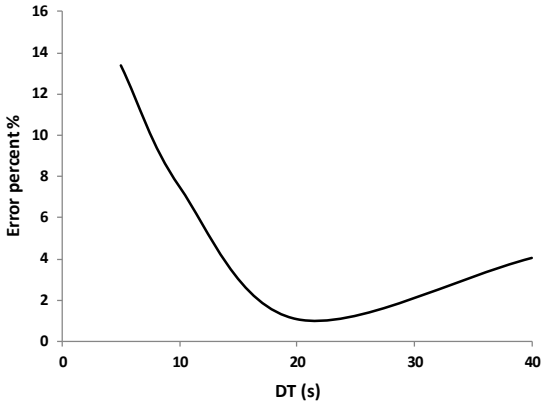

Fig. 11, Error between experimental and FEM results for ω=1000 rpm, and x_1= 30 mm.

Figure 10 also suggests the dominance of pin-generated heat at the high-temperature zone. This result agrees with the experimental finding. However, the pin insertion point must be distant from the plate edge. The metal that comes into contact with the pin shares the same temperature. Thus, the experimental positions of the holes drilled to measure the temperature effectively indicated the maximum temperature position. In the model calculation for DT simulation, shoulder diameter alone was used. Thus, the shoulder is the main source of heat generation, and the pin stirring zone produces the peak temperature. This finding is supported by previous studies [3]. When pin-generated heat was incorporated into the simulation inputs (i.e., two heat sources, namely, the pin tip and the shoulder) during DT, the simulated peak temperature was higher than the actual temperature. This finding may be attributed to the weak forces on the pin when the shoulder was in contact with the work-piece. Moreover, the value of the friction coefficient on the pin surface area decreased because of the highly plasticized material.

The stirring process was difficult to simulate because of its non-linear effect on heat amount and heat distribution among mechanical forces, friction coefficient, and plastic deformation. Thus, this study only presents the heat effect on plastic strain and material displacement. Before 12 s at a depth of 1 mm, force was strengthened in the pin penetration stage. At this specific time, this force begins to stabilize. Furthermore, the temperature was less than 30% that of T_m. The sensitivity of material rate response, whether dependent or independent, was not assumed following Bachmaier et al. [25]. The effects of x_1 distance on plastic strain and material displacement at the indicated time are shown in Fig 12. This figure suggests that plastic strain increased by 47% when the initial plunging position shifted from x_1 = 30 mm to x_1 = 4 mm.

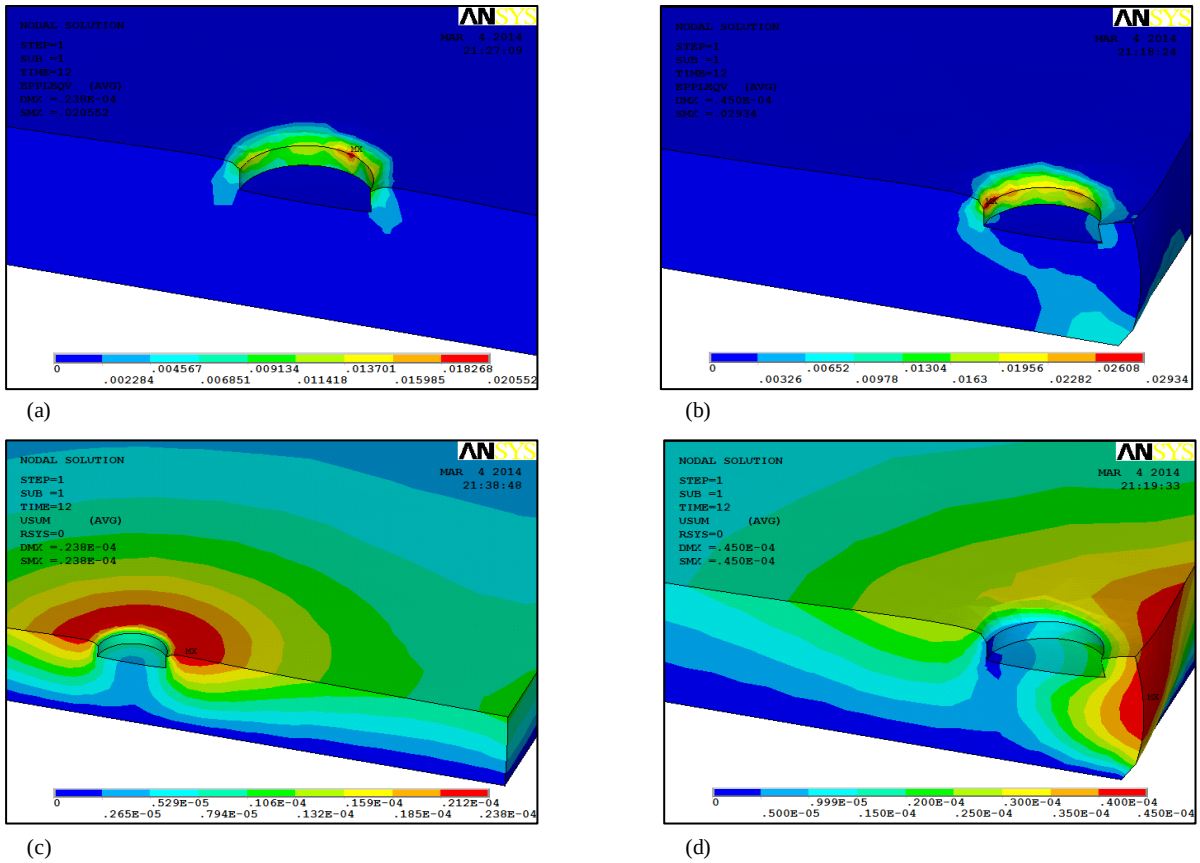

Fig. 12, FEM results. a and b: plastic strain, c and d: material displacement, for x_1 = 30 & 5 mm, respectively, at the time = 12s of the plunging stage.

Figure 13 presents the actual deformation that occurs at the plate edge, in which the unwelded zones and the end-hole defect should be either cut or repaired. The groove defect shown in Fig. 13 is caused by the temperature change when the tool moves along the welding line [4]. The use of the suggested backup plates for the tool provides three important advantages. First, the plates help eliminate unwelded zones and end-hole defects. Second, these plates facilitated sound welding by generating a constant temperature along the welding line. When tool penetration temperature was low as a result of penetration into the tool backup plate, the movement of this tool reduced the temperature depending on the welding speed [16]. More regular temperatures

resulted in uniform thermal and residual stresses along the welding line. Third, the maximum forces were generated during the penetration stage. These forces may be 35% higher than the transition forces (when the tool is moves) [20]. Thus, soft material or alloy plate can be used as a tool backup plate. These plates can be utilized multiple times.

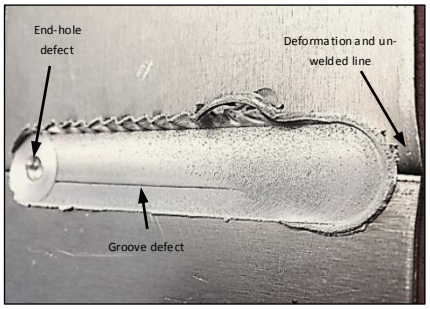

Fig. 13, Conventional defect in FSW.

5- Conclusion

The results presented in this work reveal that temperature significantly increased when the tool penetration point was near the work-piece edge. The deformation along this edge was also highly affected by that heat. The distance between the heat generation source (tool) and plate edge can significantly affect temperature values and distribution. When the distance was set at $x_1 = 30$ mm, the temperature start to stabilize, and no deformation was observed on the plate edge. Furthermore, changes in temperature were reported in the literature [4, 16] and related to weld speed alone. Thus, to enhance the accuracy of the FSW/FSP resultant temperature, the effect of the tool position from the plate edge must be ascertained.

The proposed method, using two tool backup plates, can be used to generate a constant temperature profile along the welding/processing line, prevent initial and final defects, and weaken the associated plunging forces when these plates were made from soft material.

A 3D transient heat transfer model was successfully developed to predict the temperature at different plunging distances and DTs. The thermomechanical model was also established to determine the effect of heat on plastic strain and material displacement.

References

[1] B. T. Gibson, D. H. Lammlein, T. J. Prater, W. R. Longhurst, C. D. Cox, M. C. Ballun, K. J. Dharmaraj, G. E. Cook, and a. M. Strauss, "Friction stir welding: Process, automation, and control," *J. Manuf. Process*, vol. 16, no. 1, pp. 56–73, Jan. 2014.

[2] L. E. Murr, "A Review of FSW Research on Dissimilar Metal and Alloy Systems," *J. Mater. Eng. Perform*, vol. 19, no. 8, pp. 1071–1089, , Feb. 2010.

[3] Ø. Frigaard, Ø. Grong, and O. T. Midling, "A process model for friction stir welding of age hardening aluminum alloys," *Metall. Mater. Trans. A*, vol. 32, no. 5, pp. 1189–1200, 2001.

[4] R. Nandan, G. G. Roy, and T. Debroy, "Numerical Simulation of Three-Dimensional Heat Transfer and Plastic Flow During Friction Stir Welding," *Metall. Mater. Trans. A*, vol. 37A, pp. 1247–1259, 2006.

[5] M. Dehghani, a. Amadeh, and S. a. a. Akbari Mousavi, "Investigations on the effects of friction stir welding parameters on intermetallic and defect formation in joining aluminum alloy to mild steel," *Mater. Des.*, vol. 49, pp. 433–441, Aug. 2013.

[6] K. Kimapong and T. Watanabe, "Lap Joint of A5083 Aluminum Alloy and SS400 Steel by Friction Stir Welding," *Mater. Trans.*, vol. 46, no. 4, pp. 835–841, 2005.

[7] R. S. Mishra and Z. Y. Ma, "Friction stir welding and processing," *Mater. Sci. Eng. R Reports*, , vol. 50, no. 1–2, pp. 1–78, Aug. 2005.

[8] W. D. Pilkey, and D. F. Pilkey. *Stress Concentration Factor*. New Jersey, USA: John Wiley & Sons Inc, pp.148, 2008.

[9] Y. Uematsu, K. Tokaji, Y. Tozaki, T. Kurita, and S. Murata, "Effect of re-filling probe hole on tensile failure and fatigue behaviour of friction stir spot welded joints in Al–Mg–Si alloy," *Int. J. Fatigue*, vol. 30, no. 10–11, pp. 1956–1966, Oct. 2008.

[10] R. S. Mishra, M. W. Mahoney. *Friction Stir Welding and processing*. USA: ASM International, pp.223, 2007.

[11] Y. X. Huang, B. Han, Y. Tian, H. J. Liu, S. X. Lv, J. C. Feng, J. S. Leng, and Y. Li, “New technique of filling friction stir welding,” *Sci. Technol. Weld. Join.*, vol. 16, no. 6, pp. 497–501, Aug. 2011.

[12] C. M. Chen and R. Kovacevic, “Finite element modeling of friction stir welding—thermal and thermomechanical analysis,” *Int. J. Mach. Tools Manuf.*, vol. 43, no. 13, pp. 1319–1326, Oct. 2003.

[13] H.-S. Mun and S.-I. Seo, “Welding strain analysis of friction stir-welded aluminum alloy structures using inherent strain-based equivalent loads,” *J. Mech. Sci. Technol.*, vol. 27, no. 9, pp. 2775–2782, Sep. 2013.

[14] P. Heurtier, M. J. Jones, C. Desrayaud, J. H. Driver, F. Montheillet, and D. Allehaux, “Mechanical and thermal modelling of Friction Stir Welding,” *J. Mater. Process. Technol.*, vol. 171, no. 3, pp. 348–357, Feb. 2006.

[15] M. Song and R. Kovacevic, “Thermal modeling of friction stir welding in a moving coordinate system and its validation,” *Int. J. Mach. Tools Manuf.*, vol. 43, no. 6, pp. 605–615, May 2003.

[16] D. Jacquin, B. de Meester, a. Simar, D. Deloison, F. Montheillet, and C. Desrayaud, “A simple Eulerian thermomechanical modeling of friction stir welding,” *J. Mater. Process. Technol.*, vol. 211, no. 1, pp. 57–65, Jan. 2011.

[17] X. . Zhu and Y. . Chao, “Numerical simulation of transient temperature and residual stresses in friction stir welding of 304L stainless steel,” *J. Mater. Process. Technol.*, vol. 146, no. 2, pp. 263–272, Feb. 2004.

[18] J. Luis, P. Castellanos, and A. Rusinek, "Temperature Increase Associated with Plastic Deformation Under Dynamic Compression: Application to Aluminium Alloy AL 6082,". *Journal of Theoretical and Applied Mechanics.*, vol. 50, no. 2, pp. 377-398, 2012.

[19] V. Soundararajan, S. Zekovic, and R. Kovacevic, “Thermo-mechanical model with adaptive boundary conditions for friction stir welding of Al 6061,” *Int. J. Mach. Tools Manuf.*, vol. 45, no. 14, pp. 1577–1587, Nov. 2005.

[20] D. Trimble, J. Monaghan, and G. E. O’Donnell, “Force generation during friction stir welding of AA2024-T3,” *CIRP Ann. - Manuf. Technol.*, vol. 61, no. 1, pp. 9–12, Jan. 2012.

[21] H. Schmidt, J. Hattel, and J. Wert, “An analytical model for the heat generation in friction stir welding,” *Model. Simul. Mater. Sci. Eng.*, vol. 12, no. 1, pp. 143–157, Jan. 2004.

[22] B.L. Juneja. *Fundamentals of Metal Forming Processes*. India: New Age International Publishers, pp. 19, 2010.

[23] Y. J. Chao, S. Liu, and C. Chien, “Friction stir welding of al 6061-T6 thick plates: Part II - numerical modeling of the thermal and heat transfer phenomena,” *J. Chinese Inst. Eng.*, vol. 31, no. 5, pp. 769–779, Jul. 2008.

[24] B. M. Tweedy, C. A. Widener, J. D. Merry, J. M. Brown, and D. A. Burford, “Factors affecting the properties of swept friction stir spot welds,” *proceeding of the SAE SP world congress*, (Detroit), Technical Paper, vol. 2196, pp. 11, 2008.

[25] A. Bachmaier, M. Hafok, and R. Pippan, “Rate Independent and Rate Dependent Structural Evolution during Severe Plastic Deformation,” *Mater. Trans.*, vol. 51, no. 1, pp. 8–13, 2010.